Nanomaterials induce different levels of oxidative stress, depending on the used model system: Comparison of *in vitro* and *in vivo* effects

Isabel Karkossa
Helmholtz-Zentrum fur Umweltforschung UFZ https://orcid.org/0000-0003-2781-1877
Anne Bannuscher
Bundesinstitut fur Risikobewertung
Bryan Hellack
IUTA
Wendel Wohlleben
BASF SE
Julie Laloy
University of Namur
Miruna S. Stan
University of Bucharest
Anca Dinischiotu
University of Bucharest
Martin Wiemann
IBE R&D
Andreas Luch
Bundesinstitut fur Risikobewertung
Andrea Haase
Bundesinstitut fur Risikobewertung
Martin von Bergen
Helmholtz-Zentrum fur Umweltforschung UFZ
Kristin Schubert (kristin.schubert@ufz.de)
Helmholtz-Centre for Environmental Research - UFZ https://orcid.org/0000-0003-4365-084X

Research

Keywords: Nanomaterials, Omics, Mode of Action, STIS, Instillation, Alveolar epithelial cells, Alveolar macrophages

Posted Date: January 11th, 2021

DOI: https://doi.org/10.21203/rs.3.rs-57664/v2

Version of Record: A version of this preprint was published at Science of The Total Environment on August 1st, 2021. See the published version at https://doi.org/10.1016/j.scitotenv.2021.149538.

Abstract

Background: The immense variety and constant development of nanomaterials (NMs) raise the demand for a facilitated risk assessment, for which knowledge on NMs mode of actions (MoAs) is required. For this purpose, a comprehensive data basis is of paramountcy that can be obtained using omics. Furthermore, the establishment of suitable *in vitro* test systems is indispensable to follow the 3R concept and to master the high number of NMs. In the present study, we aimed at comparing NM effects *in vitro* and *in vivo* using a multi-omics approach. We applied an integrated data evaluation strategy based on proteomics and metabolomics to four silica NMs and one titanium dioxide-based NM. For *in vitro* investigations, rat alveolar epithelial cells (RLE-6TN) and rat alveolar macrophages (NR8383) were treated with different doses of NMs, and the results were compared to effects on rat lungs after short-term inhalations and instillations at varying doses with and without a recovery period.

Results: Since the production of reactive oxygen species (ROS) is described to be a critical biological effect of NMs, and enrichment analyses confirmed oxidative stress as a significant effect upon NM treatment *in vitro* in the present study, we focused on different levels of oxidative stress. Thus, we found opposite changes for proteins and metabolites that are related to the production of reduced glutathione in alveolar epithelial cells and alveolar macrophages, illustrating that NMs MoAs depend on the used model system. Interestingly, *in vivo,* pathways related to inflammation were affected to a greater extent than oxidative stress responses. Hence, the assignment of the observed effects to the levels of oxidative stress was different *in vitro* and *in vivo* as well. However, the overall classification of “active” and “passive” NMs was consistent *in vitro* and *in vivo*.

Conclusions: The consistent classification indicates both tested cell lines to be suitable for NM toxicity assessment even though the induced levels of oxidative stress strongly depend on the used model systems. Thus, the here presented results highlight that model systems need to be carefully revised to decipher the extent to which they can replace *in vivo* testing.

2. Background

The high variability of nanomaterials (NMs) physico-chemical properties renders them valuable for a wide range of applications, e.g. cosmetics, textiles, packaging, electronics and medical devices [1]. Moreover, new NM variants are continuously developed and previous studies have shown that especially silica or titanium dioxide NMs are among those with the highest production volumes of 5,500 – 2400,000 t and 3,000 – 88,000 t worldwide per year, respectively [2, 3, 4, 5]. This makes a detailed characterization of their possible health effects indispensable.

So far, regulatory risk assessment mainly depends on *in vivo* testing, even though animal tests are time-consuming, costly, and ethically questionable. However, replacing animal tests by *in vitro* assays is challenging. Up to now much afford has been undertaken to develop integrated approaches to testing and assessment (IATAs) combining several *in chemico, in vitro*, and *in vivo* tests in a structured manner,

employing specific decision trees [6]. The development of IATAs is strongly connected to the development of Adverse Outcome Pathways (AOPs) [7], and insights into the mode of actions (MoAs) are of utmost importance for the latter. Omics approaches can provide extensive information about cellular responses to NMs. Among the various omics techniques, in praxis, transcriptomics reveals the most comprehensive information, but proteomics and metabolomics are closer to the phenotype [8, 9, 10]. The shortcomings of single omics techniques can be overcome by integrating multiple omics into one mechanistic oriented analysis, and we have previously shown that using several omics approaches facilitates unraveling NMs MoAs [11, 12], helps to develop NM grouping strategies, and to identify relevant physico-chemical properties [11, 12]. Here, we focused on NMs MoAs *in vitro* and *in vivo* and on the transferability of both approaches.

Since the lung is considered the main entry portal for airborne NMs [13], we investigated effects on the lung *in vitro* and *in vivo*. If NMs reach the alveoli, they can be cleared by macrophages, which can phagocytose NMs [14]. Inside the alveoli, epithelial cells form a barrier between the gas phase and blood circulation [15, 16] and can take up NMs [17, 18, 19, 20]. By transcytosis through the epithelial cells, NMs may travel into the interstitial space, from where they can enter the lymph nodes and the blood circulation, thus leading to possible adverse effects in secondary organs [21, 22, 23, 24]. Hence, alveolar macrophages and alveolar epithelial cells are relevant model systems to investigate NM effects *in vitro*, and well established rat cell lines of alveolar macrophages (NR8383) and alveolar epithelial type II cells (RLE-6TN) were used in the present study to analyze the effects of four silica-based NMs (SiO2_15_Amino, SiO2_15_Unmod, SiO2_7 and SiO2_40) as well as one titanium dioxide-based NM (TiO2_NM105). While SiO2_15_Amino and SiO2_15_Unmod are precipitated NMs, SiO2_40 and SiO2_7 are pyrogenic (fumed). Furthermore, the effects that were observed *in vitro* were compared to those *in vivo* to investigate the applicability of these *in vitro* model systems for NM risk assessment.

For this purpose, short-term inhalation studies (STIS) and intratracheal instillation studies with rats were used, since both were shown to be suitable to classify NMs [25, 26]. Due to short follow up periods, both methods focus on the detection of early adverse effects, such as inflammation or beginning histological changes. Importantly, both methods have advantages and disadvantages. While STIS reflect the physiological way of NMs entering the lung as an aerosol, instillations are easier to handle, and the actual dose delivered to the lung is highly reliable. Also, an administration of particles via instillation requires a vehicle, in which the NMs need to be suspended. This vehicle may alter the physico-chemical properties of the NMs and influence their distribution in the lung [27]. However, the instillation approach provides particles at a high dose rate, which is more similar to most *in vitro* approaches. Therefore, both techniques were applied in the present study, followed by proteomics and metabolomics analyses on lung samples of the rats.

One major biological effect of NMs is reported to be the formation of reactive oxygen species (ROS), which may result in inflammation, possibly leading to adverse effects [28]. The formation of ROS and the emergence of adverse effects depends on the physico-chemical properties of the used NMs, but the detailed mechanisms are not fully understood, yet [28, 29]. Especially metal oxide-based NMs can induce

the formation of ROS due to the release of transition metals. Furthermore, the presence of pro-oxidative functional groups or the binding of environmental contaminants to the NM surface can support the production of ROS, thus affecting their toxicity [30]. Under normal conditions, these ROS can be neutralized by anti-oxidants, but if the ROS levels increase beyond the neutralization capacity, oxidative stress emerges [31]. To describe the different levels of oxidative stress, a stratified oxidative stress model has been developed [32, 33, 34, 35]. This tiered model describes the dependence of the oxidative stress level on the ratio of reduced glutathione (GSH) to oxidized glutathione (GSSG). GSH is an anti-oxidant, which is oxidized to GSSG during its neutralization of ROS. Under normal conditions, the GSH/GSSG ratio is high. However, it decreases with over-proportional increases of ROS, a process whose biological consequences may be described by three tiers: In tier 1 nuclear factor erythroid 2-related factor 2 (Nrf2) target genes such as anti-oxidants are formed, followed by inflammation reactions mediated by nuclear factor kappa-light-chain-enhancer of activated B cells (Nfκb) and activator protein 1 (Ap-1) in tier 2, and cytotoxicity in tier 3 [29, 32, 33]. Since the level of oxidative stress highly influences the formation of adverse effects upon NM treatment [36, 37], we aimed at a detailed analysis of the levels of oxidative stress by integrative omics analysis. Furthermore, we compared *in vitro* and *in vivo* results to clarify to which extent animal tests could be replaced by cellular experiments in future risk assessment.

3. Results

To get insights into NMs MoAs, the effects of four silica NMs (SiO2_15_Unmod, SiO2_15_Amino, SiO2_40, SiO2_7) and TiO2_NM105 were investigated *in vitro* and *in vivo*. The physico-chemical properties of these NMs have been described before [11, 12, 25, 38, 39, 40], and a summary of their key physico-chemical properties is presented in Table 1.

3.1 *In vitro* investigations

First, the effects of these five NMs were investigated *in vitro* in alveolar type II cells and alveolar macrophages at three different doses after an exposure time of 24 h. Changes of protein (Additional file 2: Figure S1 – Figure S4) and metabolite (Additional file 2: Figure S5 – Figure S8) abundances were considered relative to untreated controls and the summary of the percentages of significantly ($p.adj \leq 0.05$) altered proteins and metabolites (Figure 1a) shows that significant changes appeared for metabolites only at the highest investigated dose (10 µg/cm^2 for TiO2_NM105 and 50 µg/cm^2 for the other tested NMs) in type II cells. Interestingly, the pyrogenic SiO2_40 and SiO2_7, as well as TiO2_NM105, were the only NMs, which significantly affected metabolites also at a dose of 10 µg/cm^2 in type II cells and macrophages, where none of the other tested NMs resulted in significant alterations (Additional file 2: Figure S5 – Figure S8). TiO2_NM105 showed significantly changed metabolites at a dose of 10 µg/cm^2 in type II cells but not in macrophages. In contrast, almost no significantly altered proteins were observable in type II cells, while dose-dependent increases of the portion of significantly altered proteins were noticeable for SiO2_40 and SiO2_7 after treatment of macrophages. Thus, in

accordance with our previous studies, SiO2_40, SiO2_7, and TiO2_NM105 were considered “active” NMs [11, 12], while SiO2_15_Unmod and SiO2_15_Amino were classified as “passive”.

Additionally, exposure times of 6 h and 48 h were investigated for type II cells. After 6 h of NM treatment, a maximum of 72 significantly altered proteins was observable for 10 µg/cm^2 SiO2_7, compared to 220 and 462 proteins under the same conditions but after 24 h and 48 h incubation, respectively (Additional file 1: Table E3). Thus, the 6 h time point was excluded from further analyses.

An enrichment analysis was applied to the significantly (p.adj ≤ 0.05) altered proteins and metabolites, which showed mainly enrichment of pathways that are related to oxidative stress, e.g. mitochondrial dysfunction, Nrf2-mediated oxidative stress response and oxidative phosphorylation (Additional file 2: Figure S9). Thus, we focused on the investigation of the levels of oxidative stress that were reached under the tested conditions. For this purpose, we used only results after 24 h treatment because only minor time-dependent changes were observable between 24 h and 48 h (Additional file 2: Figure S9 and Figure S10).

3.1.1 GSH/GSSG signaling

Since the level of GSH is highly connected to the formation of oxidative stress, proteins and metabolites that are linked to GSH/GSSG signaling [41, 42, 43, 44, 45, 46, 47] were examined first (Figure 1b). In type II cells (Figure 1b, left), SiO2_40, SiO2_7, and TiO2_NM105 were the only NMs that induced significant changes after treatment with 10 µg/cm^2, which is the dose we used in previous screening experiments with twelve NMs in type II cells as well [11]. Interestingly, SiO2_15_Unmod and SiO2_15_Amino showed the same trends, with SiO2_15_Unmod leading to higher elevations (expressed as Log2(fold changes), Log2(FCs)) than SiO2_15_Amino. Overall, the NM treatment of type II cells led to increased abundances of proteins and metabolites that are part of the GSH/GSSG signaling, thus indicating an increased production of GSH, especially in case of SiO2_40, SiO2_7, and TiO2_NM105, confirming that not only SiO2_40 and SiO2_7 are “active” NMs but also TiO2_NM105, which is consistent with our previous study [11].

Interestingly, the opposite effects were observed for macrophages (Figure 1b, right) compared to type II cells (Figure 1b, left). Most significant changes were obtained for SiO2_7 and SiO2_40 at the highest investigated dose of 10 µg/cm^2. SiO2_15_Unmod showed the same trends, even though with less significance. The decreased abundances of proteins and metabolites suggest a decreased GSH production for these three NMs in macrophages. This, in turn, may have led to an insufficient neutralization of appearing ROS, thus inducing further oxidative stress reactions. The opposite changes in type II cells and macrophages occurred predominantly in the treatment with 10 µg/cm^2 SiO2_7 (Figure 1c).

3.1.2 Comparison of oxidative stress levels

To clarify whether the observed effects on the GSH/GSSG signaling for the two cell lines led to a different assignment to the three tiers of oxidative stress, the changes of proteins and metabolites that are connected to these tiers were investigated. Specifically, induction of tier 1 is accompanied by the activation of Nrf2 targets, tier 2 by Nfκb and Ap-1 targets, and tier 3 by cytotoxicity [29, 32, 33].

Interestingly, all the proteins that were identified in the present study and relevant to maintain the GSH/GSSG homeostasis (Figure 1b, c) are regulated by the transcription factor Nrf2 [48, 49, 50, 51], the hallmark of tier 1. Thus, the NMs presumably led to tier 1 in the used type II cells at the highest applied dose of 10 µg/cm^2 for TiO2_NM105 and 50 µg/cm^2 for the other NMs. In macrophages, decreased abundances of analytes that are connected to GSH/GSSG signaling were observed for SiO2_7, SiO2_40, and SiO2_15_Unmod, suggesting that these three NMs led to a decreased GSH/GSSG ratio, while SiO2_15_Amino and TiO2_NM105 did not.

Besides the proteins that are part of the GSH/GSSG signaling, Gstm1, Nqo1, Hmox1, Txn, Txnrd1, Cat, Sod1, Sod2 and Lamp2 have been described to be Nrf2 targets [48, 49, 52] and thus appear relevant for tier 1 (Figure 2a).

To investigate, whether also tier 2 was induced, the data were screened for Nfκb and Ap-1 target genes and hence, inflammatory processes. Importantly, several of the already described Nrf2 target genes have also a binding position for Nfκb or Ap-1. Examples are Gclc, Idh, Pgd, Phgdh, Hmox1, Nqo1, Cat, Sod2, and Lamp2 [53, 54]. Furthermore, Icam1 [55, 56], Il18 [57, 58], B2m [59], Tnfaip8 [60], and Bax [61, 62] have been described to be target genes of Nfκb or Ap-1 and related to either inflammation or apoptosis. Another candidate is Ccr1, which is expressed mitogen-activated protein kinase (Mapk)-dependently [63]. Since the interactions of chemokines and chemokine receptors are relevant for the migration of immune cells, the Ccr1 is an important candidate to investigate whether tier 2 was induced. Furthermore, it has been shown that lack of Ccr1 leads to diminished inflammatory responses and higher mortality in mice [64].

Finally, candidates reflecting tier 3 and thus cytotoxicity were examined. Besides Bax [65], which was assigned to tier 2 in the present study because it is an Nfκb target protein [61, 62], also Vdac1 is involved in the formation of mitochondrial pores and thus in the induction of apoptosis [66] and should consequently be assigned to tier 3. Furthermore, it has been shown that an increased citric acid cycle (TCA) leads to the increased formation of ROS, followed by apoptosis [67]. Besides the already mentioned proteins, Glud1, and Fh are involved in the TCA [68, 69] and were thus assigned to tier 3. In addition, sphingomyelins (SMs), which belong to the class of sphingolipids and are mainly found in plasma membranes and lipoproteins, are relevant for the formation of ROS. SMs are hydrolyzed in response to oxidative stress, thus resulting in the formation of ceramides, which act as second messengers that are involved in the induction of apoptosis. Importantly, the concrete mechanisms are not fully understood, yet [70, 71]. A summary of all mentioned analytes and their assignment to the different tiers of oxidative stress can be found in Tables S1 and S2.

In type II cells, almost no significant changes were noticed for all these candidates up to the highest tested dose of 50 µg/cm^2 (Figure 2a), while treatment of macrophages with 10 µg/cm^2 SiO2_40 and SiO2_7 led to significant alterations. Importantly, SiO2_15_Unmod again showed the same trends as SiO2_40 and SiO2_7, but the effects were less pronounced. Furthermore, major differences were recognizable between treated type II cells and macrophages once again, especially after treatment with 10 µg/cm^2 SiO2_7 (Figure 2b). For type II cells, significant changes appeared only in proteins that are Nrf2 target genes, thus confirming that in type II cells only tier 1 of oxidative stress was affected under the tested conditions. The significantly affected proteins were Sod1, Txn, Gstm1, and Lamp2. In contrast, the used macrophages led to significant changes over all tiers after treatment with 10 µg/cm^2 SiO2_7. Interestingly, there are several cases in which opposite changes in protein abundance were visible in type II cells and macrophages. Examples are Sod1 and Sod2 with opposite changes among themselves and additionally, opposite changes in the two investigated cell lines. The fact that Sod1 and Sod2 resulted in different directions of alteration can be explained by their localization within the cell. While Sod1 can be found in the cytoplasm, Sod2 is responsible for neutralizing ROS in the mitochondria. Furthermore, both proteins have not only an Nrf2 binding site but also an Nfκb binding site in their promoter region. While the Nfκb binding site in Sod1 has been described to be relatively insensitive, the binding site in Sod2 seems to be highly sensitive [72], thus suggesting the Sod1 expression to be predominantly induced by Nrf2, while the Sod2 expression may be induced by Nfκb. This is a piece of additional evidence that type II cells led only to tier 1, whereas in macrophages all three tiers were initiated.

3.2 Comparison of *in vivo* and *in vitro* results

Next, we aimed to investigate the *in vivo* effects of SiO2_7 and TiO2_NM105 using STIS and of SiO2_15_Amino, SiO2_15_Unmod, SiO2_7, and SiO2_40 applying instillations. For both methods, changes in lung proteome and metabolome were investigated at several doses. Exposure groups (E) were sacrificed directly after treatment for 5 d or 3 d in STIS and instillations, respectively. In contrast, recovery groups (R) had a recovery time of 21 d after the treatment period. The percentages of significantly altered proteins (Additional file 2: Figure S11 – Figure S14) and metabolites (Additional file 2: Figure S15 – Figure S18) indicated dose-dependent increases of significantly altered analytes mainly for STIS exposure groups (Figure 3a). Thereby, the most significant changes appeared for 50 mg/m^3 TiO2_NM105 in STIS exposure groups. Importantly, this dose was only used for the exposure groups, while TiO2_NM105 was tested only up to a dose of 10 mg/m^3 in the recovery groups. Besides, the effects of SiO2_7 were assessed only up to a dose of 5 mg/m^3 in exposure and recovery groups.

Instillations were performed up to a dose of 0.36 mg in exposure and recovery groups for all four assessed NMs. The results show that SiO2_7 and SiO2_40 induced no significantly altered metabolites under any of the conditions. In contrast, for the supposedly less “active” NMs SiO2_15_Amino and SiO2_15_Unmod, a high amount of significantly altered metabolites was ascertained. Since the increased numbers of significantly altered proteins for SiO2_7 and SiO2_40 compared to the other two NMs

indicated more substantial effects for SiO2_7 and SiO2_40, the lack of changes within the metabolome might be explained by overwhelming effects that were not reproducibly detectable any longer.

Notably, the assignment to the three tiers of oxidative stress *in vivo* was not as clear (Figure 3b) as for the *in vitro* results, even though significant changes were observable for all three tiers, especially in the case of SiO2_7, SiO2_40, and TiO2_NM105, indicating those to be “active” *in vivo*. Furthermore, analytes with dose-dependent changes were detectable, e.g. Ornithine, Sod1, Sod2, and Txn.

The different results of the assignment to the three tiers *in vitro* and *in vivo* may be explained by the cellular composition of rat lungs (Figure 4a), with only 14.2% alveolar type II epithelial cells and 3% alveolar macrophages [73] and the circumstance that the two cell types investigated within the present study showed opposite effects. The comparison of Log2(FC) distributions of analytes that are connected to the three tiers of oxidative stress after treatment with SiO2_7 *in vitro* and *in vivo* (Figure 4b) exemplifies this. For GSH/GSSG signaling, opposite effects were obtained for type II cells and macrophages, but no clear trends were observed in STIS and instillations. Analytes connected to the three tiers revealed no clear trends either. However, the higher distribution ranges (Figure 4b) indicated elevated changes in macrophages and STIS, suggesting these model systems to be more sensitive.

Since the GSH/GSSG signaling did not reflect many of the significant changes *in vivo* (Figure 3a), Ingenuity Pathway Analysis (IPA, Qiagen) was used to identify NM effects *in vivo*. This analysis confirmed that oxidative stress pathways like glutathione redox reactions I, Nrf2-mediated oxidative stress response, and mitochondrial dysfunction were not among the most significantly enriched pathways (Additional file 2: Figure S19). Furthermore, chemokine signaling was found to be enriched mainly in the case of the instillation studies with SiO2_7 and SiO2_40 (Figure 4c). Examples for pathways with higher enrichment were endocytosis signaling, phagosome maturation, leukocyte extravasion signaling, remodeling of epithelial adherens junctions, integrin signaling, and actin cytoskeleton signaling. Apoptosis signaling was again mainly enriched for SiO2_7 and SiO2_40 in the instillation studies, thus indicating that these two NMs had the most potent effects. Interestingly, most pathways showed more significant enrichment in the recovery groups than in the exposure groups. The complete results from the enrichment analysis can be found in Additional file 1 (Table E25 – E30).

Since SiO2_7 was investigated using STIS and instillations, the results obtained with this NM can be used for the comparison of these two methods, where differences were observable. Notably, most of the candidates, which showed differences were not significantly altered. Exceptions are Txn, Grb2, Glud1, and Vdac1, which were significantly increased with one method and significantly decreased with the other. However, on the pathway level, the results between STIS and instillations were mostly comparable.

In summary, these results indicate the same classification of NMs *in vitro* and *in vivo*, although biological effects differed. SiO2_7, SiO2_40, and TiO2_NM105 were classified to be “active”, while SiO2_15_Amino led to almost no changes, thus suggesting it to be “passive”. SiO2_15_Unmod induced the same trends as SiO2_7 and SiO2_40, thus indicating that it might have adverse effects at higher doses.

4. Discussion

In the present study, we aimed to analyze the MoAs of a set of five NMs (SiO2_15_Unmod, SiO2_15_Amino, SiO2_7, SiO2_40, and TiO2_NM105) *in vitro* and *in vivo*. Thereby, we focused on the tiers of oxidative stress [32, 33, 34, 35] that are induced in the different model systems upon treatment with the NMs at various doses. For *in vitro* toxicity assessment, alveolar type II cells and alveolar macrophages were used. Both originated from rats to assure comparability to the conducted STIS and instillations. In order to obtain detailed information on the occurring effects, proteomics and metabolomics were applied.

Importantly, SiO2_7 and SiO2_40 were classified to be “active” in all four model systems *in vitro* and *in vivo*, thus confirming our previous classification based on *in vitro* data [11, 12]. Since SiO2_15_Unmod generally revealed the same trends as SiO2_7 and SiO2_40, even though with less significance, it should be classified “active” as well. This is in accordance with the literature, where it has been shown that SiO2_15_Unmod is “active” *in vitro* [38] and *in vivo* [25, 74]. Importantly, SiO2_15_Amino was classified to be “passive” based on all conducted studies, which has been described before as well [11, 25, 38]. This illustrates that the used surface modification can influence the effects since the only difference between SiO2_15_Unmod and SiO2_15_Amino are amino groups on the surface of latter, which is in accordance to the literature [74]. Furthermore, it suggests that the route of production may affect NM toxicity because SiO2_15_Amino and SiO2_15_Unmod, which resulted in fewer effects, are precipitated silica NMs, while SiO2_7 and SiO2_40 are fumed. The observation that fumed NM variants can be more reactive than precipitated ones has been described before as well [75]. Interestingly, the results of the present study indicated TiO2_NM105 to be “active” in type II cells but “passive” in macrophages, which is in contrast to its former classification as “active” in the same cell line of alveolar macrophages, which was based on the toxicological endpoints [38]. Furthermore, it was shown to be “active” *in vivo* before [25]. Thus, the macrophages possibly underestimated the TiO2_NM105 effects, while the type II cells resulted in a classification that is in accordance with previously published data. Notably, the release of lactate dehydrogenase (LDH), a marker for cytotoxicity in alveolar macrophages, was also considerably lower in the present study (Additional file 2: Table S2) compared to the previous study classifying TiO2_NM105 “active” based on toxicological endpoints (LDH, glucuronidase, tumor necrosis factor) [38]. One possible explanation for this observation might be the use of different TiO2_NM105 batches, while the experimental setup was the same here. Since the focus of the present study was on oxidative stress, it has to be mentioned that in the previous study also ROS releases were assessed, which changed not dose-dependently. Notably, also SiO2_15_Amino and SiO2_15_Unmod were investigated in this study, of which only SiO2_15_Unmod resulted in significantly altered ROS releases and assignment to “active” NMs [38], which is in line with the here presented data. The fact that differences in the formation of oxidative stress between the two supposedly “active” NMs TiO2_NM105 and SiO2_15_Unmod were described in macrophages before [38] and also observed here, in particular in GSH/GSSG signaling, indicates different MoAs for the two NMs. These results suggest that TiO2_NM105 is possibly not utilizing oxidative stress-related pathways in macrophages. However, the observed discrepancy in the classification of TiO2_NM105 highlights that care should be taken when classifying NMs since various

factors, like the model system, the experimental setup, and the type of assessed parameters affect the final classification.

Importantly, our main focus was to assign the observed effects to the tiers of a previously described stratified oxidative stress model [32, 33, 34, 35]. This assignment revealed that the same NMs could induce different tiers of oxidative stress in dependency of the used model system. Since the induction of the tiers of oxidative stress mainly depends on the GSH/GSSG ratio, we focused on GSH/GSSG signaling first. While the “active” NMs led to increased abundances for proteins and metabolites that are related to the GSH/GSSG signaling, decreased abundances were observable in macrophages. This suggests that upon NM treatment, the type II cells triggered the production of GSH, to be able to neutralize the appearing ROS, thus protecting themselves from too high levels of oxidative stress and further damage, which has been observed before in type II cells after treatment with different materials [76, 77]. In contrast, the decreased GSH/GSSG signaling in macrophages indicated decreased GSH levels, which have been described before as well and were explained by a NM-induced release of GSH or an increased requirement for GSH [78, 79]. Importantly, the results presented here instead suggest a decreased GSH production. These opposite effects on the GSH/GSSG signaling subsequently led to differences for analytes that can be assigned to the tiers of oxidative stress. Since all proteins described here to be necessary for the production of GSH and NADPH are regulated by Nrf2 [48, 49, 50, 51], we concluded that in type II cells only tier 1 was affected by the NM treatments but not the following tiers. In contrast, for macrophages, significant changes were recognizable for the “active” NMs over all three tiers.

Differences in the oxidative status of NM-treated cells have been described before for epithelial cells and macrophages, where the depletion of GSH was observed for both cellular systems depending on the tested NM. Thereby, either the transformation of GSH to GSSG was hypothesized to be responsible for the GSH depletion or cell membrane damages resulting in GSH leakage [80]. A possible explanation for the differences in the oxidative status upon NM treatment of macrophages and epithelial cells lies in the mechanisms of oxidative stress induction in both. In contrast to epithelial cells, macrophages are well-known for their ability to induce a respiratory burst upon phagocytosis of foreign substances, leading to the production of ROS, involved in pathogen killing or degradation. Furthermore, they can act as second messengers inducing pathways related to Nfκb, Ap-1, Mapk, and phosphatidylinositol 3-kinase (Pi3k) [81]. Additionally, macrophages carry receptors, e.g. Fc receptors, scavenger receptors (SRs), and toll-like receptors (TLRs), that can bind specific types of NMs. Recognition of NMs by TLRs and SRs, for instance, can lead to the activation of macrophages, inducing inflammatory processes [82]. Besides, the activation of TLRs can result in the recruitment of mitochondria to phagosomes and elevated production of mitochondrial ROS [83]. Hence, in macrophages, several potential mechanisms are available that can trigger ROS and subsequent effects, which are not available in epithelial cells, probably accounting for the different effects observed for the two cell lines. Also, differences in the experimental setup may have affected the NM-induced effects. While the alveolar macrophages were exposed to the NMs under serum-free conditions, the treatment of alveolar type II cells was performed with the presence of serum, thus influencing the surface reactivity, the uptake of the NMs, and potentially the biological effects.

While the *in vitro* results allowed for an exact assignment to the tiers of oxidative stress, this concept was not transferable to the *in vivo* results (Figure 3). This might be because the lung consists of various cell types (Figure 4a) that may display different effects upon NM exposure. Another reason might be that the actually deposited doses calculated for the here applied experimental setup elsewhere (Additional file 2: Table S5) [84] using the Multiple-Path Particle Dosimetry (MPPD) model [85, 86], relate to *in vitro* doses, which did not induce many significant changes in type II cells and macrophages. However, an enrichment analysis with proteins and metabolites was conducted (Figure 4c) to get an overview on the cellular processes, showing that the typical pathways that are related to the tiers of oxidative stress (glutathione redox reactions, Nrf2-mediated oxidative stress response, mitochondrial dysfunction, chemokine signaling, apoptosis signaling) were not among the most significantly enriched pathways. In contrast, pathways related to inflammatory processes like endocytosis signaling, phagosome maturation, leukocyte extravasation signaling, remodeling of epithelial adherens junctions, integrin signaling, and actin cytoskeleton signaling played a major role. The circumstance that inflammatory processes rather than oxidative stress responses were observable *in vivo* suggests that either (i) oxidative stress was not detectable because of the differences in the various cells within the lung or (ii) that the oxidative stress responses already turned into inflammatory responses at the investigated time point or (iii) that the inflammatory processes were not induced via oxidative stress but different pathways. Furthermore, it was observed that the recovery groups exhibited a more significant enrichment of pathways than the exposure groups, indicating that NM exposure might lead to long-term effects, which needs to be evaluated in further studies.

Besides differences in exposure and recovery groups, also slight differences between STIS and instillations conducted with SiO2_7 were observed. One might argue that this is due to a divergence of deposited dose in STIS and instillations, but these are comparable. The deposited dose for the 5 mg/m^3 inhaled SiO2_7 was calculated to relate to 0.06 µg/cm^2 and 0.07 µg/cm^2 for exposure and recovery groups, respectively (Additional file 2: Table S5) [84]. In contrast, for instillations, the complete deposition of NMs is assumed. Thus, the applied 0.36 mg SiO2_7 relate to 0.06 µg/cm^2 considering the rat lung to have a surface of 5571 cm^2 [87]. Consequently, the observed differences appear probably due to the methods themselves and not the deposited doses. Notably, on the pathway level, the results were comparable, indicating comparisons on the pathway level to be better suitable when applying different model systems.

Taken together, the integrated omics data show that depending on the *in vitro* model system distinct and even opposite biological responses to the same NM can be detected. Alveolar macrophages seem to be a more sensitive *in vitro* model system as they have shown stronger responses. Therefore, and in line with the 3R concept, they provide a valuable tool in acute toxicity testing. Overall, it appears that the *in vitro* models inadequately reflected the *in vivo* situation. However, it must not be overlooked that a 24 h exposure of selected cell types to NMs cannot reflect what is happening in the complex lung after several days of exposure. Signaling pathways may be switched on or off rapidly, cell types will interact and respond differently. Bearing this in mind, it is important to underline that the classification of “active” and

“passive” NMs was largely congruent between the tested model systems and also compared to previous studies. Thus, omics are generally suitable to distinguish “active” and “passive” NMs, with the major advantage that they additionally allow mechanistic insights, which cannot be accomplished investigating toxicological endpoints.

5. Conclusions

In summary, we show that NM-induced cellular effects can lead to a different assignment to the tiers of oxidative stress, which strongly depends on the used model system. Opposite effects on the GSH/GSSG signaling were observable in type II cells and macrophages, with type II cells leading to an increased GSH production and thus only tier 1 and macrophages displaying a decreased GSH production and significant changes over all three tiers. Hence, it was not surprising that the assignment was not as clear for the *in vivo* results of rat lungs that consist not only of type II cells and macrophages but also of type I cells, endothelial cells and interstitial cells. However, the *in vitro* and *in vivo* results were consistent regarding the classification of the tested NMs, thus indicating that both tested cell lines are suitable to assess NM toxicity. Since the macrophages exhibited more significant changes over all tiers of oxidative stress, they might be a more sensitive model system. Taken together, the presented results illustrate that the MoAs of NMs vary in different model systems and given that, care needs to be taken when using biomarkers for NM risk assessment.

6. Methods

6.1 Selected NMs and NM dispersion

SiO2_15_Amino and SiO2_15_Unmod (both precipitated) were provided in suspension by BASF SE. SiO2_7 and SiO2_40 (both pyrogenic) were manufactured by Evonik Industries and provided as powders. TiO2_NM105 was obtained as powder from the JRC repository. The physico-chemical properties for these NMs were described in detail earlier [11, 12]. A summary of selected properties can be found in Table 1. Before use, NMs were dispersed by an indirect probe sonication protocol [88] as described before [11, 12].

6.2 Study design and selected doses

The applied study design is depicted in Additional file 2: Figure S20 to point out the experimental setup (model systems, investigated NMs, applied doses, exposure times) and any previous publication of the obtained data. In summary, NM effects were investigated *in vitro* using rat alveolar type II cells (RLE-6TN) and rat alveolar macrophages (cell line NR8383). Thereby, proteins and metabolites were obtained from individual samples. For insights into NM effects *in vivo*, short-term inhalation studies (STIS) and instillations were performed with rats. STIS were conducted using doses up to 50 mg/m^3, which has been described before to relate to 11.9-23.8 µg/cm^2 *in vitro,* assuming a deposition of approximately 5-10 % [89]. Accordingly, *in vitro* studies were conducted with 0.1-50 µg/cm^2, depending on the cytotoxicity of the

tested NMs in the two cell lines, which have been described previously for the used NMs in alveolar type II cells [11] and alveolar macrophages [12] and summarized in Additional file 2 (Table S1 and Table S2). Instillations were conducted with 0.09-0.36 mg NM supposing that the full dose was deposited. For STIS and instillations, proteins and metabolites were extracted from the lungs of the same animals.

6.3 Cell culture

Cell culture of alveolar macrophages (cell line NR8383, ATCC, CRL-2192, USA) [12, 38] and alveolar type II cells (cell line RLE-6TN, ATCC, CRL-2300, USA) [11] was conducted as described before to achieve optimal comparability to previous studies. Details can be found in Additional file 2.

Macrophages were exposed to 45, 22.5 and 11.25 µg/mL of SiO2_15_Amino, SiO2_15_Unmod, SiO2_40, SiO2_7, and TiO2_NM105 for 24 h under serum-free conditions. Thus, nominal doses assuming complete sedimentation were 10, 5, and 2.5 µg/cm^2. The results obtained with this experimental setup for selected proteins and metabolites were previously published [12] (Additional file 2: Figure S20). Type II cells were treated with 1, 10, or 50 µg/cm^2 silica NMs for 24 h and 48 h, respectively. TiO2_NM105 was investigated at doses of 0.1, 1 and 10 µg/cm^2 due to its high cytotoxicity. The TiO2_NM105 results were briefly described in one of our previous studies [11] (Additional file 2: Figure S20). Untargeted proteomics were additionally conducted after 6 h of treatment.

For macrophages, three to four replicates were used for metabolomics and four replicates for proteomics. In the case of type II cells, the metabolomics approach was conducted in four replicates, while proteomics was performed in four to five replicates.

6.4 Short-term inhalation studies (STIS)

STIS were conducted with SiO2_7 and TiO2_NM105 under agreement «UN 18 306 DO», approved by the Committee on the Ethics of Animal Experiments of the University of Namur. The procedure was described before [84]. Briefly, female Wistar rats (Charles River, France) were exposed to the nanoaerosols for 6 h/d over 5 consecutive days or to filtered air (controls) and either sacrificed immediately after exposure (exposure groups, E) or 21 d after exposure (recovery groups, R) by a Nembutal intraperitoneal injection of (60 mg/kg) (Ceva Sante Animale, France). For each group, five rats were used. The lungs were directly frozen in liquid nitrogen and used for proteomics and metabolomics. The metabolomics results have been published before [84] (Additional file 2: Figure S20) but were re-analyzed here. Since more effects were observable for SiO2_7 than TiO2_NM105 during the *in vitro* studies, STIS were conducted with 0.5, 2, and 5 mg/m^3 SiO2_7 in both exposure and recovery groups. TiO2_NM105 was investigated at doses of 0.5, 2, and 10 mg/m^3 in exposure as well as recovery groups, not leading to many significant changes. Hence, in addition, 50 mg/m^3 were tested in the exposure group.

6.5 Instillation studies

The experimental design for intratracheal instillation with SiO2_15_Amino, SiO2_15_Unmod, SiO2_7, and SiO2_40 was approved by The Ethics Committee of the “Vasile Goldis” Western University of Arad and authorized by the National Sanitary Veterinary and Food Safety Authority of Romania with registration no. 007/27.11.2017. The applied procedure has been previously described [84]. In brief, male Wistar rats from “Cantacuzino” National Institute of Research (Bucharest, Romania) were exposed to 0.36, 0.18, and 0.09 mg NM in PBS for 3 d (exposure groups, E) and directly sacrificed afterwards or after an additional recovery time of 21 d (recovery group, R). For each group, four rats were used. The lungs were directly frozen in liquid nitrogen and used for proteomics and metabolomics. The metabolomics results have been published before [84] (Additional file 2: Figure S20) but were re-analyzed here.

6.6 Sample Preparation for Omics Studies

For the *in vitro* samples, the preparation was conducted as described before [11, 12]. Thereby, metabolites and proteins were extracted from individual samples. In brief, to isolate proteins, RIPA buffer containing 0.05 M Tris/HCl (pH 7.4, Roth, Germany), 0.15 M NaCl (Roth, Germany), 0.001 M EDTA (Roth, Germany), 1 % Igepal (Sigma Aldrich, Germany), 0.25 % Na-deoxycholate (Sigma Aldrich, Germany), 10 mM Na-Pyrophosphate (Sigma Aldrich, Germany), 10 mM β-Glycerolphosphate (Sigma Aldrich, Germany), 1 mM Sodiumorthovanadate (Sigma Aldrich, Germany), 10 µl/ml Protease-inhibitor (Merck Millipore, USA), 10 µl/ml β-Mercaptoethanol, 10 µl/ml NaF, and 2 µl/ml Na was added to the washed cells. Next, samples were shaken (10 min, 4 °C), cell debris were collected, samples were frozen at -80 °C, thawed, rotated (30 min, 4 °C), and centrifuged (30 min, 12000 g, 4 °C). The protein concentration was determined using Bradford assay (Bio-Rad, USA). In contrast, metabolites were extracted by addition of 5 % chloroform, 45 % methanol, 50 % water with subsequent rotation (30 min, 4 °C) and centrifugation (10 min, 500 g, 4 °C).

After STIS and instillations, the frozen lungs were homogenized as described before [84], and proteins, as well as metabolites, were extracted from the lungs of the same rats according to the *in vitro* studies.

6.7 Targeted Metabolomics and untargeted Proteomics

The here presented metabolomics data were published before [84] but re-evaluated in analogy to the proteomics data (Additional file 2: Figure S20). In brief, the AbsoluteIDQ p180 Kit (Biocrates, Austria) was used as described previously [11, 12, 84, 90], and samples were analyzed with an API 5500 triple quadrupole mass spectrometer (ABSciex, Germany), coupled to an Agilent 1260 Infinity HPLC system (Agilent, USA). Analyst® software and MetIDQ were used for data analysis. The subsequent analysis was performed as described before [11, 12], where the resulting metabolite concentrations were normalized to the respective cell numbers, and values below the limit of detection were excluded. Fold changes (FCs, treatment vs. control) of the average values were used for further analyses.

For untargeted proteomics, tandem mass tag (TMT)-labeling (Thermo Scientific, USA) was applied. Therefore, 25 µg protein per sample were used, and labeling was conducted with 0.1 mg label.

For type II cells, the workflow was conducted according to the manufacturer's instructions and as described before [11, 91, 92]. For these samples, TMT-6-plex (Thermo Scientific, USA) was used, while for all other sample sets TMT-10-plex (Thermo Scientific, USA) was applied.

Effects on macrophages were investigated as described previously [12]. In brief, paramagnetic beads were used, which lead to improved sample quality and allow for fractionation [93, 94]. The paramagnetic bead approach was also applied to the samples from the *in vivo* studies.

As described before [11, 12], labeled samples were analyzed on a nano-UPLC system (Ultimate 3000, Dionex, USA) with trapping column (Acclaim PepMap 100 C18, 3 µm, nanoViper, 75 µm × 5 cm, Thermo Fisher, Germany) and analytical column (Acclaim PepMap 100 C18, 3 µm, nanoViper, 75 µm × 25 cm, Thermo Fisher, Germany). For peptide separation, a non-linear gradient of 150 minutes was applied. Eluted peptides were ionized using a chip-based ESI source (Nanomate, Advion, USA), coupled to the mass spectrometer (QExactive HF, Thermo Scientific, USA). MS raw data were processed using ProteomeDiscoverer 2.2. The database search was performed against the UniprotKB reference proteome of *Rattus norvegicus* (27 February 2019), resulting in replicate FCs (treatment versus control), which were log2-transformed and median normalized before further analyses.

6.8 Statistical Analysis

Statistical analysis of log2-transformed FCs was performed in R-3.5.0 with the use of several packages [95, 96, 97, 98, 99, 100, 101, 102, 103, 104]. To unravel significant changes compared to controls, the Student's t-test with Benjamini & Hochberg adjustment was performed for proteins and metabolites that were quantified in at least three biological replicates. FCs and adjusted p-values (p.adj) for all data sets can be found in the Additional file 1 (Table E3 – E10) together with replicate values and calculation results (Table E11 – E24).

Enrichment analyses were performed using Ingenuity Pathway Analysis (IPA, Qiagen, Germany) [105, 106]. For this purpose, the data were filtered for significantly ($p.adj \leq 0.05$) altered analytes, the lung was selected as tissue and the rat as organism. The used mapping of metabolites to identifiers from the Human Metabolome Database (HMDB) that was used for this analysis can be found in the Additional file 1 (Table E2), where also the Uniprot Accession mapping to genes is stored (Table E1). Furthermore, the obtained IPA results are summarized in Table E25 – E30 for all data sets.

7. Declarations

7.1 Ethics approval and consent to participate

STIS were conducted under agreement «UN 18 306 DO», approved by the Committee on the Ethics of Animal Experiments of the University of Namur. The experimental design for intratracheal instillation was approved by The Ethics Committee of the “Vasile Goldis” Western University of Arad and authorized by the National Sanitary Veterinary and Food Safety Authority of Romania with registration no. 007/27.11.2017.

7.2 Consent for publication

Not applicable

7.3 Availability of data and materials

The proteomics and metabolomics datasets generated from alveolar macrophages are available at Zenodo under following DOI: https://doi.org/10.5281/zenodo.3514213.

The proteomics raw data have been deposited to the ProteomeXchange Consortium via the PRIDE [107] partner repository with following dataset identifiers: PXD020289 (alveolar type II cells), PXD020158 (alveolar macrophages), PXD020178 (STIS), and PXD020184 (instillations).

Reviewer account details:

Alveolar type II cells:

Username: reviewer29642@ebi.ac.uk

Password: TiQCUbdO

Alveolar macrophages:

Username: reviewer85083@ebi.ac.uk

Password: nRGN6jSe

STIS:

Username: reviewer31171@ebi.ac.uk

Password: 7MwHlUpR

Instillations:

Username: reviewer76333@ebi.ac.uk

Password: Ns9JRyNS

7.4 Competing interests

The authors declare that they have no competing interests.

7.5 Funding

This project is part of the SIINN ERA-NET and is funded under the ERA-NET scheme of the Seventh Framework Program of the European Commission, BMBF Grant Agreement No. 03XP0008. The STIS performed at the University of Namur were funded by the BfR (grant agreement number 1329-561).

7.6 Authors' contributions

The study was planned by KS, AH, and MvB with contributions from AL. MvB and AH secured funding. AB conducted experiments with alveolar type II cells, while MW was responsible for studies with alveolar macrophages. STIS were performed by JL and instillations by MSS and AD. AB extracted proteins and metabolites from all samples and performed metabolomics. IK prepared and analyzed protein samples and did subsequent data analyses and statistical analyses for the metabolomics and proteomics results. BH provided NMs physico-chemical properties. IK, AB, BH, WW, JL, MSS, AD, MW, AL, AH, MvB, and KS interpreted the results. IK and KS prepared the figures. The manuscript was written by IK and KS with contributions from all co-authors.

7.7 Acknowledgements

The authors would like to take this opportunity to thank all institutions for their support of this project. In addition, the authors want to thank Maj Schuster for excellent technical assistance.

8. References

1. Stark WJ, Stoessel PR, Wohlleben W, Hafner A. Industrial applications of nanoparticles. Chem Soc Rev. 2015;44 16:5793-805.
2. Piccinno F, Gottschalk F, Seeger S, Nowack B. Industrial production quantities and uses of ten engineered nanomaterials in Europe and the world. J Nanopart Res. 2012;14 9:1109.
3. Commission E: Types and uses of nanomaterials, including safety aspects, Accompanying the Communication from the Commission to the European Parliament, the Council and the European Economic and Social Committee on the Second Regulatory Review on Nanomaterials. https://publications.europa.eu/en/publication-detail/-/publication/be32dfc7-1499-4328-b54f-a9f024805f59/language-en (2012). Accessed 07.06.2019.
4. Keller AA, McFerran S, Lazareva A, Suh S. Global life cycle releases of engineered nanomaterials. J Nanopart Res. 2013;15 6:1692.

5. Holden PA, Klaessig F, Turco RF, Priester JH, Rico CM, Avila-Arias H, et al. Evaluation of exposure concentrations used in assessing manufactured nanomaterial environmental hazards: are they relevant? Environmental science & technology. 2014;48 18:10541-51; doi: 10.1021/es502440s.
6. OECD: REPORT ON CONSIDERATIONS FROM CASE STUDIES ON INTEGRATED APPROACHES FOR TESTING AND ASSESSMENT (IATA), ENV/JM/MONO(2018)25, Series on Testing and Assessment No. 289. vol. ENV/JM/MONO(2018)252018.
7. OECD: Proposal for a template and guidance on developing and assessing the completeness of adverse outcome pathways. 2012.
8. Steuer AE, Brockbals L, Kraemer T. Metabolomic Strategies in Biomarker Research-New Approach for Indirect Identification of Drug Consumption and Sample Manipulation in Clinical and Forensic Toxicology? Front Chem. 2019;7:319; doi: 10.3389/fchem.2019.00319.
9. Wishart DS. Emerging applications of metabolomics in drug discovery and precision medicine. Nat Rev Drug Discov. 2016;15 7:473-84; doi: 10.1038/nrd.2016.32.
10. Costa PM, Fadeel B. Emerging systems biology approaches in nanotoxicology: Towards a mechanism-based understanding of nanomaterial hazard and risk. Toxicology and applied pharmacology. 2016;299:101-11; doi: 10.1016/j.taap.2015.12.014.
11. Karkossa I, Bannuscher A, Hellack B, Bahl A, Buhs S, Nollau P, et al. An in-depth multi-omics analysis in RLE-6TN rat alveolar epithelial cells allows for nanomaterial categorization. Part Fibre Toxicol. 2019;16 1:38; doi: 10.1186/s12989-019-0321-5. https://doi.org/10.1186/s12989-019-0321-5.
12. Bannuscher A, Karkossa I, Buhs S, Nollau P, Kettler K, Balas M, et al. A multi-omics approach reveals mechanisms of nanomaterial toxicity and structure–activity relationships in alveolar macrophages. Nanotoxicology. 2019:1-15; doi: 10.1080/17435390.2019.1684592. https://www.tandfonline.com/doi/abs/10.1080/17435390.2019.1684592.
13. Bakand S, Winder C, Khalil C, Hayes A. Toxicity assessment of industrial chemicals and airborne contaminants: transition from in vivo to in vitro test methods: a review. Inhal Toxicol. 2005;17 13:775-87. http://www.tandfonline.com/doi/pdf/10.1080/08958370500225240?needAccess=true.
14. Geiser M. Morphological aspects of particle uptake by lung phagocytes. Microsc Res Tech. 2002;57 6:512-22; doi: 10.1002/jemt.10105. https://onlinelibrary.wiley.com/doi/abs/10.1002/jemt.10105.
15. Muhlfeld C, Rothen-Rutishauser B, Blank F, Vanhecke D, Ochs M, Gehr P. Interactions of nanoparticles with pulmonary structures and cellular responses. Am J Physiol Lung Cell Mol Physiol. 2008;294 5:L817-29; doi: 10.1152/ajplung.00442.2007. https://www.physiology.org/doi/pdf/10.1152/ajplung.00442.2007.
16. Fröhlich E, Salar-Behzadi S. Toxicological assessment of inhaled nanoparticles: role of in vivo, ex vivo, in vitro, and in silico studies. Int J Mol Sci. 2014;15 3:4795-822; doi: 10.3390/ijms15034795.
17. Oberdörster G, Oberdörster E, Oberdörster J. Nanotoxicology: an emerging discipline evolving from studies of ultrafine particles. Environ Health Perspect. 2005;113 7:823-39.
18. Kreyling WG, Semmler M, Erbe F, Mayer P, Takenaka S, Schulz H, et al. TRANSLOCATION OF ULTRAFINE INSOLUBLE IRIDIUM PARTICLES FROM LUNG EPITHELIUM TO EXTRAPULMONARY

ORGANS IS SIZE DEPENDENT BUT VERY LOW. J Toxicol Environ Health A. 2002;65 20:1513-30; doi: 10.1080/00984100290071649. https://doi.org/10.1080/00984100290071649.

19. Semmler-Behnke M, Takenaka S, Fertsch S, Wenk A, Seitz J, Mayer P, et al. Efficient elimination of inhaled nanoparticles from the alveolar region: evidence for interstitial uptake and subsequent reentrainment onto airways epithelium. Environ Health Perspect. 2007;115 5:728-33.
20. Semmler M, Seitz J, Erbe F, Mayer P, Heyder J, Oberdörster G, et al. Long-Term Clearance Kinetics of Inhaled Ultrafine Insoluble Iridium Particles from the Rat Lung, Including Transient Translocation into Secondary Organs. Inhal Toxicol. 2004;16 6-7:453-9; doi: 10.1080/08958370490439650. https://doi.org/10.1080/08958370490439650.
21. Kreyling WG, Hirn S, Schleh C. Nanoparticles in the lung. Nature biotechnology. 2010;28 12:1275-6; doi: 10.1038/nbt.1735. http://dx.doi.org/10.1038/nbt.1735.
22. Stone V, Miller MR, Clift MJD, Elder A, Mills NL, Moller P, et al. Nanomaterials Versus Ambient Ultrafine Particles: An Opportunity to Exchange Toxicology Knowledge. Environ Health Perspect. 2017;125 10:106002; doi: 10.1289/EHP424. https://www.ncbi.nlm.nih.gov/pubmed/29017987.
23. Geiser M, Kreyling WG. Deposition and biokinetics of inhaled nanoparticles. Part Fibre Toxicol. 2010;7 1:2; doi: 10.1186/1743-8977-7-2. https://doi.org/10.1186/1743-8977-7-2.
24. Kreyling WG, Semmler-Behnke M, Takenaka S, Moller W. Differences in the biokinetics of inhaled nano- versus micrometer-sized particles. Accounts of chemical research. 2013;46 3:714-22; doi: 10.1021/ar300043r.
25. Landsiedel R, Ma-Hock L, Hofmann T, Wiemann M, Strauss V, Treumann S, et al. Application of short-term inhalation studies to assess the inhalation toxicity of nanomaterials. Part Fibre Toxicol. 2014;11 1:16.
26. Morimoto Y, Izumi H, Yoshiura Y, Tomonaga T, Lee B-W, Okada T, et al. Comparison of pulmonary inflammatory responses following intratracheal instillation and inhalation of nanoparticles. Nanotoxicology. 2016;10 5:607-18. https://www.tandfonline.com/doi/full/10.3109/17435390.2015.1104740.
27. Driscoll KE, Costa DL, Hatch G, Henderson R, Oberdorster G, Salem H, et al. Intratracheal instillation as an exposure technique for the evaluation of respiratory tract toxicity: uses and limitations. Toxicol Sci. 2000;55 1:24-35.
28. Fubini B, Hubbard A. Reactive oxygen species (ROS) and reactive nitrogen species (RNS) generation by silica in inflammation and fibrosis. Free Radic Biol Med. 2003;34 12:1507-16. https://www.sciencedirect.com/science/article/pii/S0891584903001497?via%3Dihub.
29. Huang Y-W, Wu C-h, Aronstam RS. Toxicity of transition metal oxide nanoparticles: recent insights from in vitro studies. Materials. 2010;3 10:4842-59.
30. Risom L, Møller P, Loft S. Oxidative stress-induced DNA damage by particulate air pollution. Mutat Res. 2005;592 1-2:119-37. https://www.sciencedirect.com/science/article/pii/S0027510705002460?via%3Dihub.

31. Sies H: Oxidative stress: Introduction in oxidative stress: In oxidative stress: oxidative stress: oxidants and antioxidant ed Sies H. 19191; pp xv-xxiv. Academic press London.
32. Nel A, Xia T, Mädler L, Li N. Toxic potential of materials at the nanolevel. Science. 2006;311 5761:622-7.
33. Li N, Xia T, Nel AE. The role of oxidative stress in ambient particulate matter-induced lung diseases and its implications in the toxicity of engineered nanoparticles. Free Radic Biol Med. 2008;44 9:1689-99.
34. Xiao GG, Wang M, Li N, Loo JA, Nel AE. Use of proteomics to demonstrate a hierarchical oxidative stress response to diesel exhaust particle chemicals in a macrophage cell line. J Biol Chem. 2003;278 50:50781-90; doi: 10.1074/jbc.M306423200. https://www.ncbi.nlm.nih.gov/pubmed/14522998.
35. Li N, Kim S, Wang M, Froines J, Sioutas C, Nel A. Use of a stratified oxidative stress model to study the biological effects of ambient concentrated and diesel exhaust particulate matter. Inhal Toxicol. 2002;14 5:459-86. https://www.tandfonline.com/doi/abs/10.1080/089583701753678571.
36. Manke A, Wang L, Rojanasakul Y. Mechanisms of Nanoparticle-Induced Oxidative Stress and Toxicity. Biomed Res Int. 2013;2013:15; doi: 10.1155/2013/942916. http://dx.doi.org/10.1155/2013/942916.
37. Mendoza RP, Brown JM. Engineered nanomaterials and oxidative stress: Current understanding and future challenges. Curr Opin Toxicol. 2019;13:74-80; doi: https://doi.org/10.1016/j.cotox.2018.09.001. http://www.sciencedirect.com/science/article/pii/S2468202018300536.
38. Wiemann M, Vennemann A, Sauer UG, Wiench K, Ma-Hock L, Landsiedel R. An in vitro alveolar macrophage assay for predicting the short-term inhalation toxicity of nanomaterials. J Nanobiotechnology. 2016;14 1:16; doi: 10.1186/s12951-016-0164-2. http://dx.doi.org/10.1186/s12951-016-0164-2.
39. Wiemann M, Vennemann A, Stintz M, Retamal Marin RR, Babick F, Lindner GG, et al. Effects of Ultrasonic Dispersion Energy on the Preparation of Amorphous SiO(2) Nanomaterials for In Vitro Toxicity Testing. Nanomaterials. 2018;9 1; doi: 10.3390/nano9010011. https://res.mdpi.com/nanomaterials/nanomaterials-09-00011/article_deploy/nanomaterials-09-00011.pdf?filename=&attachment=1.
40. Driessen MD, Mues S, Vennemann A, Hellack B, Bannuscher A, Vimalakanthan V, et al. Proteomic analysis of protein carbonylation: a useful tool to unravel nanoparticle toxicity mechanisms. Part Fibre Toxicol. 2015;12 1:36.
41. Kanehisa M, Goto S. KEGG: kyoto encyclopedia of genes and genomes. Nucleic Acids Res. 2000;28 1:27-30; doi: 10.1093/nar/28.1.27. https://www.ncbi.nlm.nih.gov/pubmed/10592173.
42. Kanehisa M. Toward understanding the origin and evolution of cellular organisms. Protein Sci. 2019;28 11:1947-51; doi: 10.1002/pro.3715. https://onlinelibrary.wiley.com/doi/full/10.1002/pro.3715.

43. Kanehisa M, Sato Y, Furumichi M, Morishima K, Tanabe M. New approach for understanding genome variations in KEGG. Nucleic Acids Res. 2019;47 D1:D590-d5; doi: 10.1093/nar/gky962.
44. Dickinson DA, Forman HJ. Cellular glutathione and thiols metabolism. Biochem Pharmacol. 2002;64 5:1019-26; doi: https://doi.org/10.1016/S0006-2952(02)01172-3. http://www.sciencedirect.com/science/article/pii/S0006295202011723.
45. Cohen G, Hochstein P. Glutathione peroxidase: the primary agent for the elimination of hydrogen peroxide in erythrocytes. Biochemistry. 1963;2 6:1420-8.
46. Meister A, Anderson ME. Glutathione. Annu Rev Biochem. 1983;52 1:711-60.
47. Richman P, Meister A. Regulation of gamma-glutamyl-cysteine synthetase by nonallosteric feedback inhibition by glutathione. J Biol Chem. 1975;250 4:1422-6.
48. Hayes JD, Dinkova-Kostova AT. The Nrf2 regulatory network provides an interface between redox and intermediary metabolism. Trends Biochem Sci. 2014;39 4:199-218; doi: https://doi.org/10.1016/j.tibs.2014.02.002. http://www.sciencedirect.com/science/article/pii/S0968000414000267.
49. Jung K-A, Kwak M-K. The Nrf2 System as a Potential Target for the Development of Indirect Antioxidants. Molecules. 2010;15 10:7266-91. https://www.mdpi.com/1420-3049/15/10/7266.
50. DeNicola GM, Chen P-H, Mullarky E, Sudderth JA, Hu Z, Wu D, et al. NRF2 regulates serine biosynthesis in non–small cell lung cancer. Nat Genet. 2015;47:1475; doi: 10.1038/ng.3421. https://doi.org/10.1038/ng.3421.
51. Morales Pantoja IE, Hu C-l, Perrone-Bizzozero NI, Zheng J, Bizzozero OA. Nrf2-dysregulation correlates with reduced synthesis and low glutathione levels in experimental autoimmune encephalomyelitis. J Neurochem. 2016;139 4:640-50; doi: 10.1111/jnc.13837. https://onlinelibrary.wiley.com/doi/abs/10.1111/jnc.13837.
52. Pajares M, Rojo AI, Arias E, Díaz-Carretero A, Cuervo AM, Cuadrado A. Transcription factor NFE2L2/NRF2 modulates chaperone-mediated autophagy through the regulation of LAMP2A. Autophagy. 2018;14 8:1310-22; doi: 10.1080/15548627.2018.1474992. https://doi.org/10.1080/15548627.2018.1474992.
53. Yang Y, Wu J, Wang J. A database and functional annotation of NF-κB target genes. Int J Clin Exp Med. 2016;9 5:7986-95.
54. Sawada R, Jardine KA, Fukuda M. The genes of major lysosomal membrane glycoproteins, lamp-1 and lamp-2. 5'-flanking sequence of lamp-2 gene and comparison of exon organization in two genes. J Biol Chem. 1993;268 12:9014-22. http://www.jbc.org/content/268/12/9014.abstract.
55. Rahman I, MacNee W. Role of transcription factors in inflammatory lung diseases. Thorax. 1998;53 7:601-12.
56. Lee IT, Yang CM. Inflammatory signalings involved in airway and pulmonary diseases. Mediators Inflamm. 2013;2013:791231; doi: 10.1155/2013/791231.
57. Li K, Wei L, Huang Y, Wu Y, Su M, Pang X, et al. Leptin promotes breast cancer cell migration and invasion via IL-18 expression and secretion. Int J Oncol. 2016;48 6:2479-87; doi:

10.3892/ijo.2016.3483. https://www.ncbi.nlm.nih.gov/pubmed/27082857.

58. Grandjean-Laquerriere A, Antonicelli F, Gangloff SC, Guenounou M, Le Naour R. UVB-induced IL-18 production in human keratinocyte cell line NCTC 2544 through NF-kappaB activation. Cytokine. 2007;37 1:76-83; doi: 10.1016/j.cyto.2007.02.020. https://www.sciencedirect.com/science/article/abs/pii/S1043466607000348?via%3Dihub.
59. Gobin SJ, Biesta P, Van den Elsen PJ. Regulation of human beta 2-microglobulin transactivation in hematopoietic cells. Blood. 2003;101 8:3058-64; doi: 10.1182/blood-2002-09-2924.
60. Niture S, Ramalinga M, Kedir H, Patacsil D, Niture SS, Li J, et al. TNFAIP8 promotes prostate cancer cell survival by inducing autophagy. Oncotarget. 2018;9 42:26884-99; doi: 10.18632/oncotarget.25529. https://www.ncbi.nlm.nih.gov/pubmed/29928491.
61. Kim SM, Lee SY, Cho JS, Son SM, Choi SS, Yun YP, et al. Combination of ginsenoside Rg3 with docetaxel enhances the susceptibility of prostate cancer cells via inhibition of NF-kappaB. Eur J Pharmacol. 2010;631 1-3:1-9; doi: 10.1016/j.ejphar.2009.12.018. https://www.sciencedirect.com/science/article/pii/S001429990901139X?via%3Dihub.
62. Huang C, Yao JY, Li ZF, Liu LY, Ni L, Song TS. [Small interfering RNA-mediated nuclear factor-kappaB P65 suppression induces apoptosis of hepatic carcinoma SMMC-7721 cells]. Nan Fang Yi Ke Da Xue Xue Bao. 2007;27 12:1841-4.
63. Ko J, Yun CY, Lee JS, Kim JH, Kim IS. p38 MAPK and ERK activation by 9-cis-retinoic acid induces chemokine receptors CCR1 and CCR2 expression in human monocytic THP-1 cells. Exp Mol Med. 2007;39 2:129-38; doi: 10.1038/emm.2007.15.
64. Domachowske JB, Bonville CA, Gao J-L, Murphy PM, Easton AJ, Rosenberg HF. The Chemokine Macrophage-Inflammatory Protein-1α and Its Receptor CCR1 Control Pulmonary Inflammation and Antiviral Host Defense in Paramyxovirus Infection. The Journal of Immunology. 2000;165 5:2677-82; doi: 10.4049/jimmunol.165.5.2677. https://www.jimmunol.org/content/jimmunol/165/5/2677.full.pdf.
65. Brunelle JK, Letai A. Control of mitochondrial apoptosis by the Bcl-2 family. J Cell Sci. 2009;122 4:437-41; doi: 10.1242/jcs.031682.
66. Madesh M, Hajnóczky G. VDAC-dependent permeabilization of the outer mitochondrial membrane by superoxide induces rapid and massive cytochrome. J Cell Biol. 2001;155 6:1003-16; doi: 10.1083/jcb.200105057.
67. Brookes PS, Yoon Y, Robotham JL, Anders MW, Sheu S-S. Calcium, ATP, and ROS: a mitochondrial love-hate triangle. Am J Physiol Cell Physiol. 2004;287 4:C817-C33; doi: 10.1152/ajpcell.00139.2004. https://www.physiology.org/doi/abs/10.1152/ajpcell.00139.2004.
68. Akram M. Citric Acid Cycle and Role of its Intermediates in Metabolism. Cell Biochem Biophys. 2014;68 3:475-8; doi: 10.1007/s12013-013-9750-1. https://doi.org/10.1007/s12013-013-9750-1.
69. Krebs HA. The history of the tricarboxylic acid cycle. Perspect Biol Med. 1970;14 1:154-70; doi: 10.1353/pbm.1970.0001. https://muse.jhu.edu/article/405199.

70. Andrieu-Abadie N, Gouazé V, Salvayre R, Levade T. Ceramide in apoptosis signaling: relationship with oxidative stress. Free Radic Biol Med. 2001;31 6:717-28.
71. Andrieu-Abadie N, Levade T. Sphingomyelin hydrolysis during apoptosis. Biochim Biophys Acta Mol Cell Biol Lipids. 2002;1585 2:126-34; doi: https://doi.org/10.1016/S1388-1981(02)00332-3. http://www.sciencedirect.com/science/article/pii/S1388198102003323.
72. Miao L, St Clair DK. Regulation of superoxide dismutase genes: implications in disease. Free Radic Biol Med. 2009;47 4:344-56; doi: 10.1016/j.freeradbiomed.2009.05.018. https://www.ncbi.nlm.nih.gov/pubmed/19477268.
73. Crapo JD, Barry BE, Gehr P, Bachofen M, Weibel ER. Cell Number and Cell Characteristics of the Normal Human Lung. Am Rev Respir Dis. 1982;126 2:332-7; doi: 10.1164/arrd.1982.126.2.332. https://www.atsjournals.org/doi/abs/10.1164/arrd.1982.126.2.332.
74. Großgarten M, Holzlechner M, Vennemann A, Balbekova A, Wieland K, Sperling M, et al. Phosphonate coating of SiO2 nanoparticles abrogates inflammatory effects and local changes of the lipid composition in the rat lung: a complementary bioimaging study. Part Fibre Toxicol. 2018;15 1:31; doi: 10.1186/s12989-018-0267-z. https://doi.org/10.1186/s12989-018-0267-z.
75. Di Cristo L, Movia D, Bianchi MG, Allegri M, Mohamed BM, Bell AP, et al. Proinflammatory Effects of Pyrogenic and Precipitated Amorphous Silica Nanoparticles in Innate Immunity Cells. Toxicol Sci. 2015;150 1:40-53; doi: 10.1093/toxsci/kfv258. https://doi.org/10.1093/toxsci/kfv258.
76. Stone V, Shaw J, Brown DM, MacNee W, Faux SP, Donaldson K. The role of oxidative stress in the prolonged inhibitory effect of ultrafine carbon black on epithelial cell function. Toxicol In Vitro. 1998;12 6:649-59; doi: https://doi.org/10.1016/S0887-2333(98)00050-2. http://www.sciencedirect.com/science/article/pii/S0887233398000502.
77. Liu R-M, Hu H, Robison TW, Forman HJ. Increased gamma-glutamylcysteine synthetase and gamma-glutamyl transpeptidase activities enhance resistance of rat lung epithelial L2 cells to quinone toxicity. Am J Respir Cell Mol Biol. 1996;14 2:192-7.
78. Boehme DS, Maples KR, Henderson RF. Glutathione release by pulmonary alveolar macrophages in response to particles in vitro. Toxicol Lett. 1992;60 1:53-60.
79. Deneke SM, Fanburg BL. Regulation of cellular glutathione. Am J Physiol Lung Cell Mol Physiol. 1989;257 4:L163-L73.
80. Wang L, Pal AK, Isaacs JA, Bello D, Carrier RL. Nanomaterial induction of oxidative stress in lung epithelial cells and macrophages. J Nanopart Res. 2014;16 9:2591; doi: 10.1007/s11051-014-2591-z. https://doi.org/10.1007/s11051-014-2591-z.
81. Gwinn MR, Vallyathan V. Respiratory burst: role in signal transduction in alveolar macrophages. Journal of Toxicology and Environmental Health, Part B. 2006;9 1:27-39. https://www.tandfonline.com/doi/full/10.1080/15287390500196081.
82. You DJ, Lee HY, Bonner JC. Macrophages: First Innate Immune Responders to Nanomaterials. In: Bonner JC, Brown JM, editors. Interaction of Nanomaterials with the Immune System. Cham: Springer International Publishing; 2020. p. 15-34.

83. West AP, Brodsky IE, Rahner C, Woo DK, Erdjument-Bromage H, Tempst P, et al. TLR signalling augments macrophage bactericidal activity through mitochondrial ROS. Nature. 2011;472 7344:476-80; doi: 10.1038/nature09973. https://doi.org/10.1038/nature09973.
84. Bannuscher A, Hellack B, Bahl A, Laloy J, Herman H, Stan MS, et al. Metabolomics profiling to investigate nanomaterial toxicity in vitro and in vivo. Nanotoxicology. 2020:1-20; doi: 10.1080/17435390.2020.1764123. https://doi.org/10.1080/17435390.2020.1764123.
85. Anjilvel S, Asgharian B. A multiple-path model of particle deposition in the rat lung. Fundamental and Applied Toxicology. 1995;28 1:41-50. https://www.sciencedirect.com/science/article/abs/pii/S027205908571144X?via%3Dihub.
86. Miller FJ, Asgharian B, Schroeter JD, Price O. Improvements and additions to the Multiple Path Particle Dosimetry model. Journal of Aerosol Science. 2016;99:14-26; doi: https://doi.org/10.1016/j.jaerosci.2016.01.018. http://www.sciencedirect.com/science/article/pii/S0021850215300860.
87. Johanson WG, Jr., Pierce AK. Lung Structure and Function with Age in Normal Rats and Rats With Papain Emphysema. The Journal of Clinical Investigation. 1973;52 11:2921-7; doi: 10.1172/JCI107488. https://doi.org/10.1172/JCI107488.
88. Taurozzi JS, Hackley VA, Wiesner MR. Ultrasonic dispersion of nanoparticles for environmental, health and safety assessment–issues and recommendations. Nanotoxicology. 2011;5 4:711-29; doi: 10.3109/17435390.2010.528846. https://www.tandfonline.com/doi/full/10.3109/17435390.2010.528846.
89. Haase A, Dommershausen N, Schulz M, Landsiedel R, Reichardt P, Krause B-C, et al. Genotoxicity testing of different surface-functionalized SiO2, ZrO2 and silver nanomaterials in 3D human bronchial models. Arch Toxicol. 2017; doi: 10.1007/s00204-017-2015-9.
90. Potratz S, Tarnow P, Jungnickel H, Baumann S, von Bergen M, Tralau T, et al. Combination of Metabolomics with Cellular Assays Reveals New Biomarkers and Mechanistic Insights on Xenoestrogenic Exposures in MCF-7 Cells. Chem Res Toxicol. 2017; doi: 10.1021/acs.chemrestox.6b00106. http://dx.doi.org/10.1021/acs.chemrestox.6b00106.
91. Wewering F, Jouy F, Wissenbach DK, Gebauer S, Blüher M, Gebhardt R, et al. Characterization of chemical-induced sterile inflammation in vitro: application of the model compound ketoconazole in a human hepatic co-culture system. Arch Toxicol. 2016:1-12.
92. Thompson A, Schafer J, Kuhn K, Kienle S, Schwarz J, Schmidt G, et al. Tandem mass tags: a novel quantification strategy for comparative analysis of complex protein mixtures by MS/MS. Anal Chem. 2003;75 8:1895-904. http://pubs.acs.org/doi/pdfplus/10.1021/ac0262560.
93. Hughes CS, Foehr S, Garfield DA, Furlong EE, Steinmetz LM, Krijgsveld J. Ultrasensitive proteome analysis using paramagnetic bead technology. Mol Syst Biol. 2014;10:757; doi: 10.15252/msb.20145625.
94. Hughes CS, Moggridge S, Muller T, Sorensen PH, Morin GB, Krijgsveld J. Single-pot, solid-phase-enhanced sample preparation for proteomics experiments. Nat Protoc. 2018; doi: 10.1038/s41596-

018-0082-x.

95. Wickham H, Bryan J: readxl: Read Excel Files. https://CRAN.R-project.org/package=readxl (2018). Accessed 10.09.2020.
96. Spiess AN: qpcR: Modelling and Analysis of Real-Time PCR Data. R package v. 1.4-1. https://CRAN.R-project.org/package=qpcR (2018). Accessed 10.09.2020.
97. Wickham H. The split-apply-combine strategy for data analysis. J Stat Softw. 2011;40 1:1-29.
98. Mahto A: splitstackshape: Stack and reshape datasets after splitting concatenated values. https://CRAN.R-project.org/package=splitstackshape (2018). Accessed 10.09.2020.
99. Wickham H, Henry L: tidyr: easily tidy data with “spread ()” and “gather ()” functions. R package version 0.8. 0. https://CRAN.R-project.org/package=tidyr (2018). Accessed 10.09.2020 2018.
100. Graffelman J: Calibrate: calibration of scatterplot and biplot axes. https://CRAN.R-project.org/package=calibrate (2013).
101. Gu Z, Gu L, Eils R, Schlesner M, Brors B. circlize implements and enhances circular visualization in R. Bioinformatics. 2014;30 19:2811-2.
102. Warnes GR, Bolker B, Bonebakker L, Gentleman R, Liaw WHA, Lumley T, et al: gplots: Various R Programming Tools for Plotting Data. https://CRAN.R-project.org/package=gplots (2016).
103. Neuwirth E: ColorBrewer palettes. https://cran.r-project.org/web/packages/RColorBrewer/index.html (2014).
104. Wickham H: ggplot2: elegant graphics for data analysis. https://ggplot2.tidyverse.org (2016).
105. Qiagen: Ingenuity Pathway Analysis. https://www.qiagenbioinformatics.com/products/ingenuity-pathway-analysis/ Accessed 05.12.2019.
106. Krämer A, Green J, Pollard J, Jr, Tugendreich S. Causal analysis approaches in Ingenuity Pathway Analysis. Bioinformatics. 2013;30 4:523-30; doi: 10.1093/bioinformatics/btt703. https://doi.org/10.1093/bioinformatics/btt703.
107. Perez-Riverol Y, Csordas A, Bai J, Bernal-Llinares M, Hewapathirana S, Kundu DJ, et al. The PRIDE database and related tools and resources in 2019: improving support for quantification data. Nucleic Acids Res. 2019;47 D1:D442-d50; doi: 10.1093/nar/gky1106.

9. Table

Table 1: Summary of key physico-chemical properties of the investigated NMs.
Shown are the core materials, the primary particle sizes (PPS) as given by the manufacturer, the surface areas as determined by BET and the agglomerate sizes determined by dynamic light scattering (DLS). The physico-chemical properties of these NMs were described before in detail [11, 12, 25, 38, 39, 40].

Name	Core Material	PPS [nm]	Surface Area (BET) [m^2/g]	Agglomerate Size in F12K with serum (DLS) [nm]
SiO2_15_Unmod	Silica	15	200	42
SiO2_15_Amino		15	200	144
SiO2_40		40	50	255
SiO2_7		8	300	275
TiO2_NM105	Titanium dioxide	21	51	3490

Figures

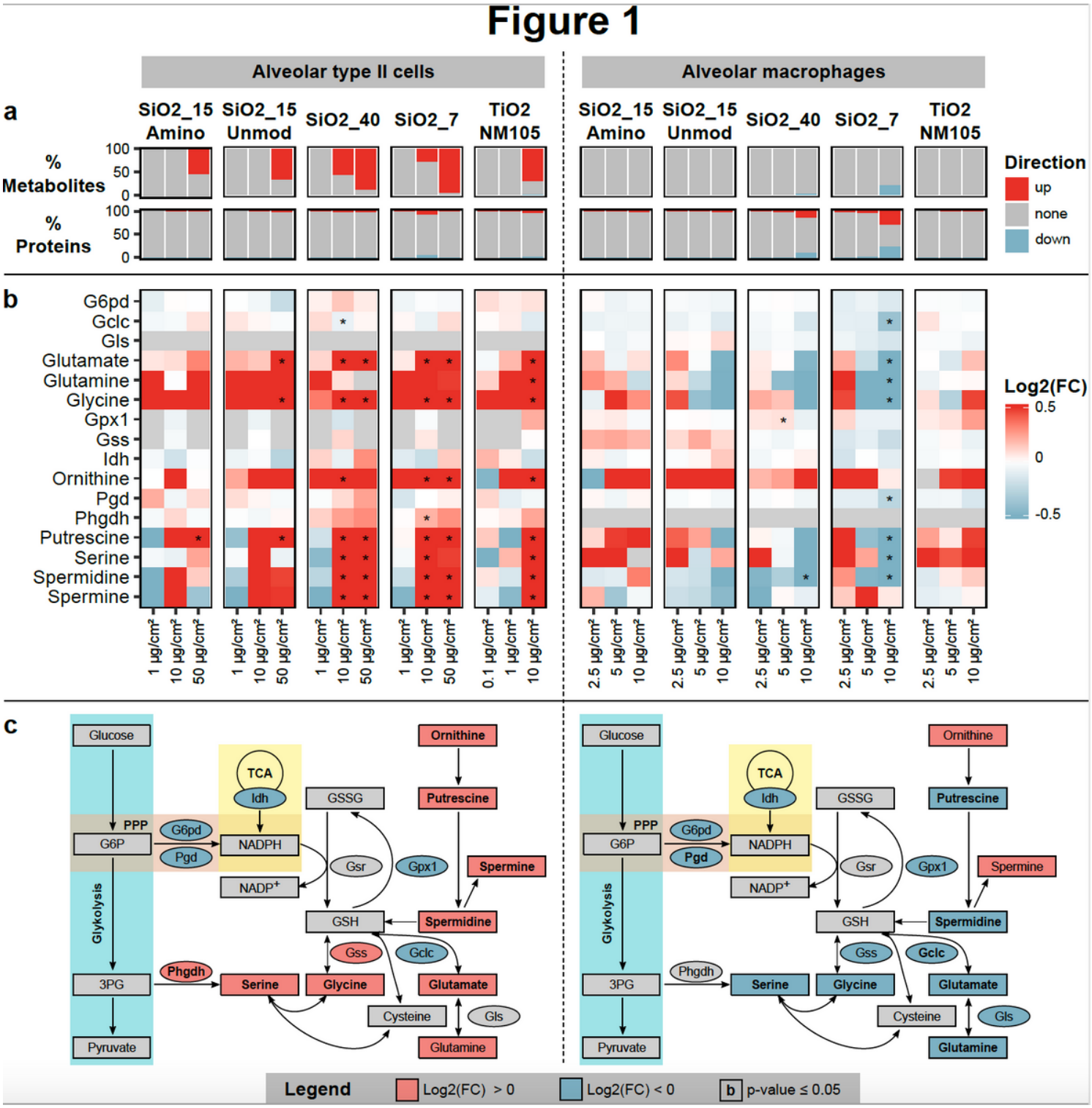

Figure 1

Summary of in vitro results with a focus on the GSH/GSSG signaling pathway. Percentages of significantly altered metabolites and proteins after exposure of type II cells (left) and macrophages (right) are shown for five different NMs that were applied at varying doses (a). The observed changes were summarized for proteins and metabolites that are connected to the GSH/GSSG signaling pathway [41, 42, 43, 44, 45, 46, 47] and significant changes (p.adj ≤ 0.05) are labeled with an asterisk (b). Furthermore,

the effects observed for the GSH/GSSG signaling pathway after treatment with 10 µg/cm2 SiO2_7 are presented, where significant changes (p.adj ≤ 0.05) are indicated with bold letters (c).

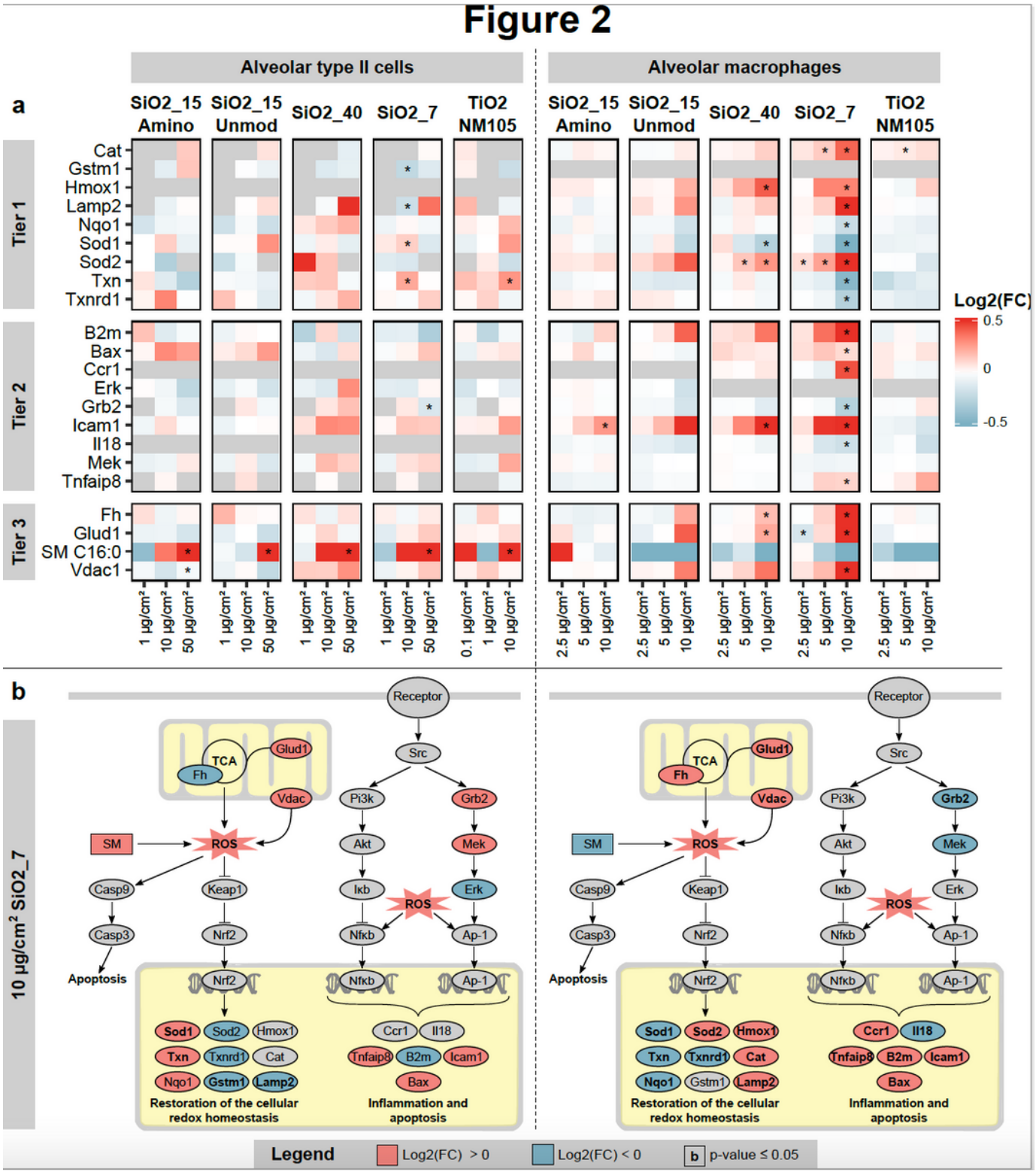

Figure 2

Summary of in vitro results with a focus on the tiers of oxidative stress. Shown are the changes after treatment of type II cells (left) and macrophages (right) with different NMs at varying doses for analytes that are connected to the tiers of oxidative stress. In tier 1, the expression of Nrf2 targets is induced. Tier 2

is accompanied by Nfκb and Ap-1 targets and thus inflammatory processes and tier 3 by cytotoxicity [29, 32, 33]. Significant changes (p.adj ≤ 0.05) are labeled with an asterisk (a). Furthermore, the effects observed for the three tiers after treatment with 10 µg/cm2 SiO2_7 are presented, and significant changes (p.adj ≤ 0.05) are indicated with bold letters (b).

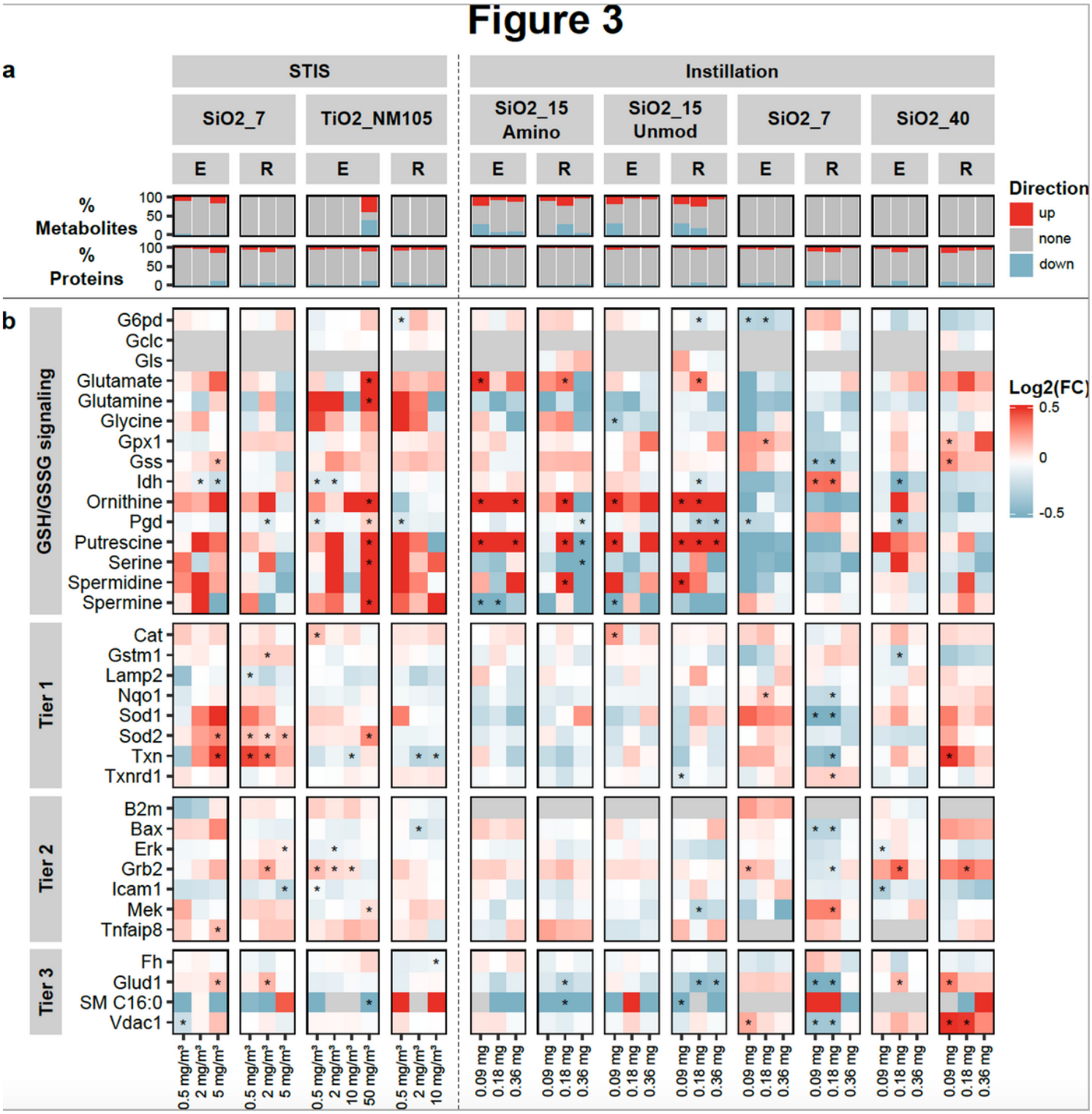

Figure 3

Summary of in vivo results with a focus on the tiers of oxidative stress. Shown are the percentages of significantly altered metabolites and proteins after STIS (left) and instillation (right) for five different NMs

that were applied at varying doses with distinguishing exposure groups (E) and recovery groups (R) (a). Furthermore, the observed changes are summarized for proteins and metabolites that are connected to the GSH/GSSG signaling pathway as well as the tiers of oxidative stress and significant changes (p.adj ≤ 0.05) are labeled with an asterisk (b).

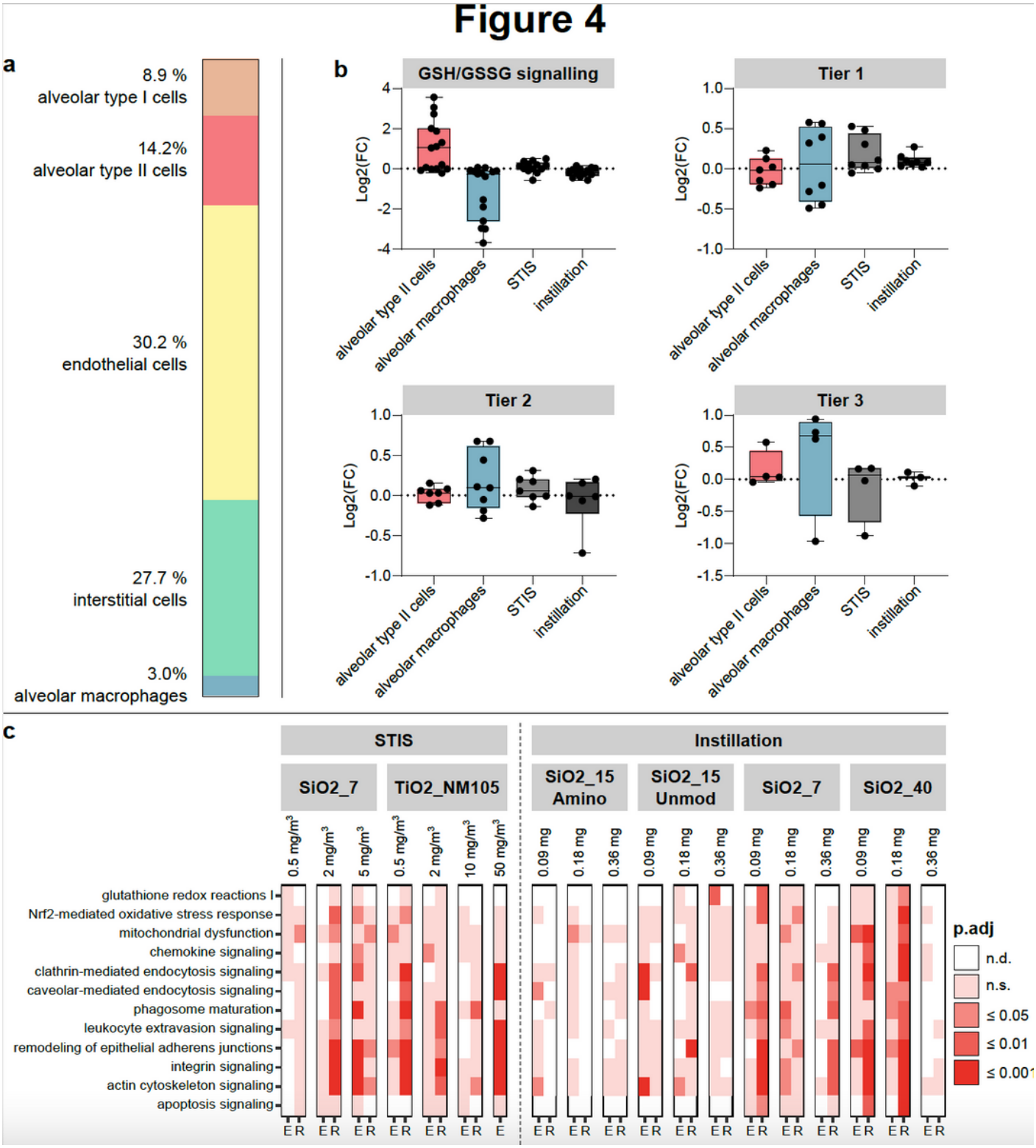

Figure 4

Classification of the in vivo results. The cellular composition of rat lungs is shown [73] (a), together with the Log2(FC) distributions for proteins (Additional file 2: Table S3) and metabolites (Additional file 2: Table S4) that are connected to the GSH/GSSG signaling or the three tiers of oxidative stress. The Log2(FC) distributions were compared for results obtained from alveolar type II cells, alveolar macrophages, STIS, and instillations. For this purpose, the values obtained for SiO2_7 were depicted since this is the NM, which was assessed with all four model systems. Thereby, in vitro doses of 10 µg/cm2 were selected, while in vivo exposure group doses of 5 mg/m3 and 0.36 mg were chosen for STIS and instillations, respectively (b). Furthermore, for a selection of IPA pathways, the adjusted p-values (p.adj) for enrichment are presented for the conducted in vivo studies at various doses and for exposure groups (E) and recovery groups (R) distinguishing between n.d. (not detected), n.s. (not significant, p.adj > 0.05), p.adj ≤ 0.05, p.adj ≤ 0.01, and p.adj ≤ 0.001 (c).

Supplementary Files

This is a list of supplementary files associated with this preprint. Click to download.

- Additionalfile1.xlsx
- Additionalfile2.pdf